



An efficiently and quickly synthesized NiO@g-C₃N₄ nanocomposite-catalyzed green synthesis of spirooxindole derivatives

Zahra Amini Moqadam¹ · Ali Allahresani² · Hassan Hassani¹

Received: 15 February 2019 / Accepted: 8 August 2019
© Springer Nature B.V. 2019

Abstract

NiO@g-C₃N₄ as an efficient catalyst for the synthesis of spirooxindole derivatives was prepared by impregnation of g-C₃N₄ with NiO nanoparticles and characterized by various techniques including thermogravimetric analysis, transmission electron microscopy, X-ray diffraction and Fourier transform infrared spectroscopy. The one-pot synthesis of spirooxindole derivatives using 1 mmol isatin, 1 mmol dimedone (or 4-hydroxycoumarin or ethyl acetoacetate) and 1 mmol malononitrile was carried out in the presence of 50 mg NiO@g-C₃N₄ in EtOH media at reflux conditions. The results showed that both series of reactions had short reaction times (less than 7 min) and high reaction efficiency (greater than 87%). Some advantages can be cited for this method, including short reaction time, excellent yields, easy workup and a reusable and inexpensive nanocatalyst.

Keywords 4-Hydroxycoumarin · Dimedone · Isatin · Malononitrile · NiO@g-C₃N₄ · Spirooxindole derivatives

Introduction

The significance of indole and its derivatives is well recognized by synthetic organic chemists and biologists [1]. The indole ring system is the most ubiquitous heterocycle in many biological systems usually found in nature [2] as well as in many compounds with pharmaceutical and biological activity [3]. Therefore, remarkable efforts have been made to synthesize analogs of di-indolyloxindoles as a variety of indole derivatives. Di-indolyloxindoles are naturally found

✉ Hassan Hassani
Hassaniir@yahoo.com

¹ Department of Chemistry, Payam Noor University, Mashhad, Iran

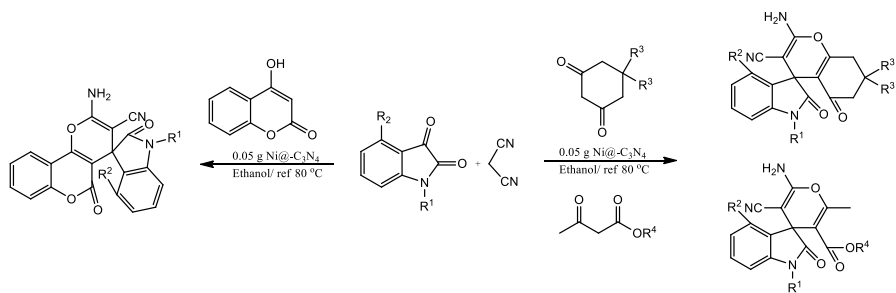
² Department of Chemistry, Faculty of Sciences, University of Birjand, P.O. Box 97175-615, Birjand, Iran

in medicinal plants and possess biological properties such as anti-inflammatory, anti-bacterial, anti-protozoal and laxative effects [4]. These compounds were prepared by the reaction of indoles with isatin or its derivatives [5], pyrazolones [6], aromatics in triflic acid [7] and other ways [8]. Despite various methods reported for the synthesis of oxindole derivatives (using a broad range of catalysts such as TfOH, Bi(OTf)₃, silica sulfuric acid, montmorillonite-K10 clay, KSF, Amberlyst-15, FeCl₃, I₂, ceric ammonium nitrate, phosphotungstic acid, ionic liquids and boron trifluoride supported on nano-SiO₂ [9]), there are still limitations for this purpose including the use of toxic solvents and heavy metals.

With the development of nanoscience and nanotechnology, nanoparticulate catalysts like metal oxides have attracted significant attention in organic transformations [10]. One possibility to expand the application of metal oxides as catalysts is to tailor their sizes in nanodimensions and consequently their surface chemistry and catalytic properties. As one of the metal oxides, nickel oxide nanoparticles have attracted much attention as inexpensive and nonhazardous catalysts or beneficial promoters that can increase the reactivity and selectivity of different organic reactions [11, 12]. A number of examples are available in the literature where nickel-based nanoparticles have been employed as catalysts during organic transformations [13, 14]. These nanoparticles may be considered as promising, safe and reusable catalysts compared to traditional catalysts because they are often recovered easily by simple workup which prevents the contamination of products [15].

A considerable challenge in handling the nanoparticles in polar solvent is the propensity of nanoparticles to aggregate rapidly into micrometer-sized particles due to van der Waal forces. The mentioned problem can be greatly resolved by decoration of nanoparticles onto the surface of supporting materials. This method significantly reduces the nanoparticles accumulation and leads to the larger surface area and superior properties for the obtained composites compared to the bare nanoparticles. In recent years, graphitic carbon nitride (g-C₃N₄) nanosheets have been known as a good candidate for supporting nanoparticles and the preparation of composite materials [16–20]. These 2D nanosheets possess advantages such as high stability in acid to alkali aqueous solutions, large surface areas, non-toxicity, easy functionalization, high thermal stability, specific physical features, simple recycling and acceptable biocompatibility [21, 22]. It is worth considering that the immobilization of metal oxide nanoparticles onto g-C₃N₄ improves the catalytic activity by advancing the charge separation at the interface of metal oxide nanoparticles' heterojunction and also by limiting the aggregation of nanoparticles [23, 24]. Recently, Allahresani et al. [25, 26] have reported a three-component synthesis of cyclic 1,3-diketones, isatin and malononitrile catalyzed by GN/SO₃H and SiO₂@g-C₃N₄.

Regarding all of the matters discussed up to now, we predicted a great catalytic performance for NiO@g-C₃N₄ nanocomposite. Thus, in this work, we report the synthesis of spirooxindole derivatives by coupling of isatin and malononitrile with cyclic-1,3-diketone or 1,3-diketoesters or 4-hydroxycoumarin using a NiO@g-C₃N₄ nanocomposite as a heterogeneous efficient catalyst via a multicomponent reaction in an aqueous medium (Scheme 1).



Scheme 1 Synthesis of spirooxindole derivatives in the presence of NiO@g-C₃N₄ nanocomposite

Experimental

Materials

All reagents were commercial reagent grade and were purchased from Merck Company and used without further purification. FT-IR spectra were recorded in the range 400–4000 cm⁻¹ on a Bruker Vector-22 FT-IR spectrometer (AVATR-370) in a KBr pellet. All NMR spectra (¹³C and ¹H) were measured at room temperature, at 250 MHz and 62.9 MHz in DMSO-d₆ using tetramethylsilane (TMS) as an internal standard, using a Bruker DPX-250 Advance instrument. X-ray diffraction (XRD) patterns are obtained from a Bruker D8-advance X-ray diffractometer with Cu K α radiation ($k = 1.5406 \text{ \AA}$). The transmission electron microscopy (TEM) images of the heterogeneous catalyst were recorded using a Philips CM10 instrument. TGA patterns of the samples were recorded using PerkinElmer Diamond TG/DTA thermal analyzer by heating the samples in an argon flow at a rate of 100 mL min⁻¹ with a heating rate of 10 °C min⁻¹, and a Mira 3TEScan-XMU scanning electron microscope was used for the scanning electron microscopy (SEM) images.

Catalyst preparation

To synthesize the NiO@g-C₃N₄ nanocomposite, in a typical procedure, fine powdered NiO (0.2 g) was well dispersed in 80 mL of deionized water for 1 h (mixture 1). Melamine (4.5 g) was also dissolved in a mixture of 5 mL of EtOH and 15 mL deionized water (mixture 2). Then, mixture 2 was added to mixture 1 and the final mixture was stirred at room temperature for 20 h. The mixture was heated at 60 °C to dryness. Finally, the prepared nanocomposite was heated in an alumina crucible with a cover in a muffle furnace at a rate of 2 °C min⁻¹ under air conditions until reaching 550 °C and held at this temperature for 4 h. The resulting black powder was ground into fine powder and stored for further use.

General procedure for one-pot synthesis of di-indolyloxindole derivatives

The NiO@g-C₃N₄ nanocomposite (0.05 mmol) was dispersed in ethanol (3 mL) for 30 min. 1 mmol dimedone (or ethyl acetoacetate or 4-hydroxycoumarin), 1 mmol malononitrile and 1 mmol isatin were added to the mixture which was stirred at reflux condition for the appropriate time, and the progress of the reaction was monitored by thin-layer chromatography. After the completion of the reaction, the crude product was extracted with ethyl acetate and dried over anhydrous Na₂SO₄. The pure products were recrystallized in hot ethanol and were identified by IR, ¹H and ¹³C NMR spectral data. NiO@g-C₃N₄ nanocomposite was separated by centrifuging, washed several times with ethanol, dried and reused for the next run.

Spectral data for selected products

2-Amino-2',5-dioxo-5,6,7,8-tetrahydrospiro-[chromene-4,30-indoline]-3-carbonitrile White solid; mp > 250 °C; IR (KBr, cm⁻¹): 33,537 (N-H), 3291 (N-H), 3171 (C-H, sp²), 2956 (C-H, sp³), 2209 (CN), 1710 (C=O), 1650 (N-C=O), 1477 (C-H, Ar); ¹H NMR (250 MHz, DMSO-d₆), ppm: 1.95 (2H, t, CH₂), 2.15 (2H, m, CH₂), 2.66 (2H, t, CH₂), 6.68 (1H, d, ArH), 6.87 (1H, t, ArH), 7.10 (1H, d, ArH), 7.22 (1H, t, ArH), 7.30 (2H, s, NH₂), 10.67 (1H, s, NH); ¹³C NMR (62.4 MHz, DMSO-d₆), ppm: 19.84, 26.82, 36.46, 46.90, 57.69, 109.204, 111.91, 117.46, 121.82, 123.30, 128.59, 134.66, 141.7, 158.75, 166.15, 178.20, 195.19.

2-Amino-7,7-dimethyl-2',5-dioxo-5,6,7,8-tetrahydrospiro-[chromene-4,30-indoline]-3-carbonitrile White solid; mp > 250 °C; IR (KBr, cm⁻¹): 3370 (N-H), 3317 (NH), 3141 (C-H, sp²), 2923 (C-H, sp³), 2196 (CN), 1728 (C=O), 1650 (N-C=O), 1605 (C-H, Ar), 1478 (C-H, Ar); ¹H NMR (250 MHz, DMSO-d₆) ppm: 0.99 (6H, s, 2CH₃), 2.15 (2H, s, CH₂), 2.47 (2H, s, CH₂), 6.75–7/25 (4H, ArH, 2H, NH₂, m), 10.31 (1H, s, NH); ¹³C NMR (62.9 MHz, DMSO-d₆), ppm: 27.49, 28.05, 32.30, 47.28, 50.463, 57.91, 109.80, 111.31, 117.71, 122.40, 123.47, 128.55, 134.86, 142.43, 152, 159.38, 164.48, 178.428, 195.27.

2-Amino-1'-benzyl-7,7-dimethyl-2,5-dioxo-5,6,7,8-tetrahydrospiro-[chromene-4,30-indoline]-3-carbonitrile White solid; mp > 250 °C; IR (KBr, cm⁻¹): 3317 (N-H), 3303 (NH), 3145 (C-H, sp²), 2917 (C-H, sp³), 2199 (CN), 1710 (C=O), 1661 (N-C=O), 1602 (C-H, Ar), 1466 (C-H, Ar); ¹H NMR (250 MHz, DMSO-d₆) ppm: 1.01 (3H, s, CH₃), 1.09 (3H, s, CH₃), 2.16–2.297 (2H, m, CH₂), 2.49 (2H, s, CH₂), 4.90 (2H, s, CH₂-Ar), 6.69 (1H, d, ArH), 6.80 (1H, t, ArH), 7.08–7.14 (2H, m, ArH), 7.17–7.330 (3H, m, ArH), 7.30 (2H, s, NH₂), 7.53 (2H, d, ArH); ¹³C NMR (62.9 MHz, DMSO-d₆) ppm: 27.35, 28.10, 32.40, 43.65, 47.07, 50.322, 57.2, 109.3, 111.2, 117.94, 123, 123.2, 127.56, 127.6, 127.72, 128.92, 133.7, 135.6, 144.5, 159.22, 165.65, 177.15, 194.95.

2-Amino-2',5-dioxo-5,6-dihydro-spiro[pyrano[3,2-c]quinoline-4,3'-indoline]-3-carbonitrile White solid; mp > 250 °C; IR (KBr, cm⁻¹): 3418 (NH), 3260 (N–H), 3140 (C–H, sp²), 2942 (C–H, sp³), 2208 (CN), 1711 (C=O), 1674 (N–C=O), 1600 (C–H, Ar), 1477 (C–H, Ar); ¹H NMR (250 MHz, DMSO-d₆), ppm: 6.75 (1H, d, ArH), 6.83 (1H, t, ArH), 7.25 (1H, d, ArH), 7.44 (1H, d, ArH), 7.49 (1H, t, ArH), 7.36 (1H, t, ArH), 7.63 (1H, d, ArH), 7.72 (2H, s, NH₂), 7.64 (1H, d, ArH), 10.85 (1H, s, NH); ¹³C NMR (62.9 MHz, DMSO-d₆), ppm: 57.24, 70.56, 101.85, 109.78, 112.76, 117.37, 117.76, 122.63, 123.10, 124.48, 125.53, 129.58, 133.63, 134.23, 142.53, 152.63, 155.58, 155.75, 158.63, 177.63.

Results and discussion

Characterizations of catalyst

The NiO@g-C₃N₄ nanocomposite was characterized by different techniques such as TGA, TEM, XRD and FT-IR.

In the case of the TGA images of g-C₃N₄, the result which is shown in Fig. 1a indicates that g-C₃N₄ is stable up to 550 °C, and after this temperature up to about 650 °C, decomposition or concentration of g-C₃N₄ nanoparticles was occurred and then stopped. Figure 1b depicts the significant decrease in the decomposition range of NiO@g-C₃N₄ toward g-C₃N₄ (occurs at 450 °C up to about 600 °C), which could be due to the presence of g-C₃N₄ stenosis connected to NiO.

As can be seen in Fig. 2a, TEM image of pure g-C₃N₄ nanosheets showed the agglomeration of the lamellar structure. According to Fig. 2b, c, NiO nanoparticles are well dispersed on the surface of g-C₃N₄ nanosheets.

The XRD patterns of g-C₃N₄ and the NiO@g-C₃N₄ nanocomposite are shown in Fig. 3a, b, respectively. The peaks at 13.1° (100) and 27.4° (002) can be related to the hexagonal phase of g-C₃N₄, according to JCPDS 087-1526, indicating in-plane repeated units and interlayer stacking peak of g-C₃N₄, respectively (Fig. 3a). Weakening of peaks at 13.1° and 27.4° in Fig. 3b reflects the reduction in the g-C₃N₄ crystallinity by the introduction of NiO nanoparticles.

As shown in Fig. 4a, the N–H bond is detected by the broad peak ranging from 3000 to 3500 cm⁻¹. The peak at 1645 cm⁻¹ belongs to heterocyclic C=N stretching vibration bond, while the C–N stretching bond of tri-s-triazine assigned by the peaks centered at 1238, 1317, 1405 and 1543 cm⁻¹. Eventually, the sharp peak at 806 cm⁻¹ is corresponding to the out-of-plane bending vibration of triazine cycle. In Fig. 4b, the peaks centered at 806, 1238, 1317, 1405 and 1543 cm⁻¹ are the peaks related to g-C₃N₄ and the peaks in the 450–550 cm⁻¹ are related to NiO.

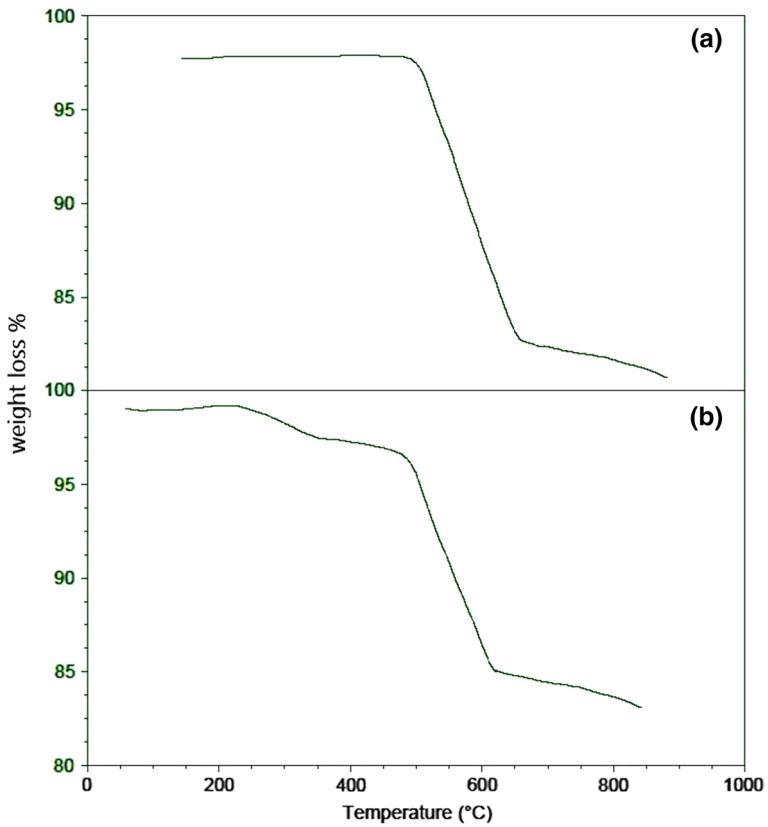


Fig. 1 TGA image of $g\text{-C}_3\text{N}_4$ (a) and $\text{NiO}@g\text{-C}_3\text{N}_4$ nanocomposite (b)

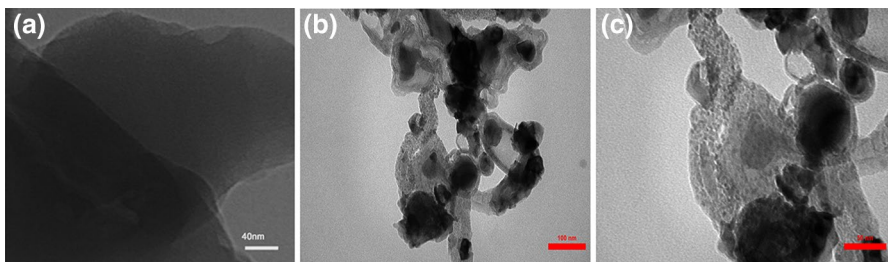


Fig. 2 TEM images of $g\text{-C}_3\text{N}_4$ (a) and $\text{NiO}@g\text{-C}_3\text{N}_4$ (b 100 nm and c 50 nm)

Catalytic activity studies

Synthesis of spirooxindole

To investigate the catalytic activity of $\text{NiO}@g\text{-C}_3\text{N}_4$ nanocomposite, the synthesis

Fig. 3 XRD images of g-C₃N₄ (a) and NiO@g-C₃N₄ (b)

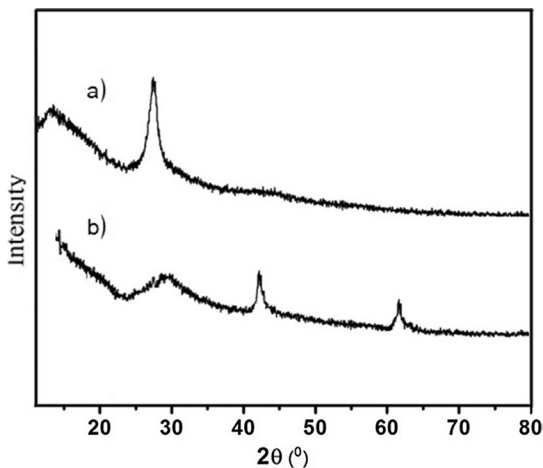
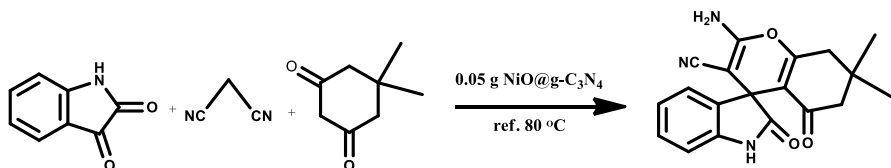
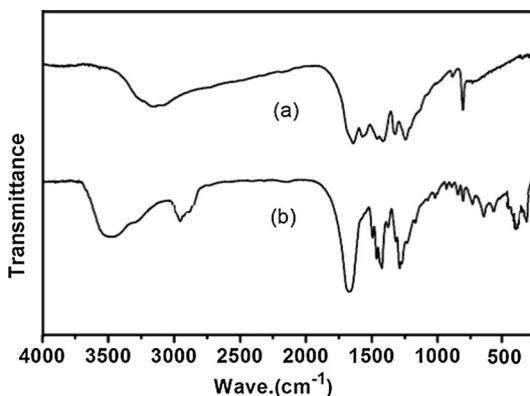


Fig. 4 FT-IR spectra of g-C₃N₄ (a) and NiO@g-C₃N₄ (b)



Scheme 2 Synthesis of spirooxindoles in the presence of a catalytic amount of SiO₂@g-C₃N₄ nanocomposite

of spirooxindole derivatives using 1 mmol of any initial compound (isatin, dime-done and malononitrile) was carried out in the presence of nanocomposite (0.05 g) as a catalyst in reflux conditions (Scheme 2).

To determine the optimal amount of the catalyst, the reaction was initially performed in the absence of catalyst, which did not produce any product after an hour (Table 1, entry 1). The control reaction in the presence of g-C₃N₄ (50 mg)

Table 1 Effect of different amounts of NiO@g-C₃N₄ nanocomposite as a catalyst on yield (%) of spirooxindole

| Entry | NiO@g-C ₃ N ₄ (g) | Time (min) | Yield ^a (%) |
|----------------|---|------------|------------------------|
| 1 | 0 | 60 | Trace |
| 2 ^b | 0.05 | 60 | Trace |
| 3 | 0.005 | 10 | 42 |
| 4 | 0.01 | 10 | 47 |
| 5 | 0.02 | 8 | 50 |
| 6 | 0.03 | 7 | 58 |
| 7 | 0.04 | 7 | 80 |
| 8 | 0.045 | 5 | 83 |
| 9 | 0.05 | 2 | 93 |
| 10 | 0.055 | 2 | 93 |

Reaction conditions: isatin (1 mmol), dimedone (1 mmol) and malonitrile (1 mmol) in the presence or the absence of catalyst in ethanol under reflux

^aIsolated yield

^bg-C₃N₄ as catalyst

as a catalyst was also carried out, and the same results were observed after an hour (Table 1, entry 2). By increasing the amount of catalyst from 5 to 50 mg, an increasing trend was observed in the percentage of the product along with the reduction in the reaction time (Table 1, entries 3–9). A further increase in catalyst content did not result in a significant change in the amount of product or reaction time (Table 1, entry 10). Therefore, 50 mg of catalyst was selected as the best value for subsequent reactions.

The reaction was performed using an optimal amount of catalyst in the presence of different solvents (Table 2). The best results were obtained in terms of product percentage and reaction time in the presence of ethanol as a solvent (Table 2, entry 1).

Table 2 Effect of different solvents on the yield (%) of spirooxindole in the presence of (0.05 g) NiO@g-C₃N₄ nanocomposite as catalyst

| Entry | Solvent | Time (min) | Yield ^a (%) |
|-------|-----------------------|------------|------------------------|
| 1 | EtOH | 2 | 93 |
| 2 | H ₂ O | 2 | 88 |
| 3 | EtOH/H ₂ O | 2 | 90 |
| 4 | CHCl ₃ | 2 | 55 |
| 5 | MeOH | 2 | 70 |
| 6 | n-Hexane | 2 | 50 |
| 7 | THF | 2 | 40 |

Reaction conditions: isatin (1 mmol), dimedone (1 mmol) and malonitrile (1 mmol) in the presence of NiO@g-C₃N₄ nanocomposite (0.05 gr) as catalyst in various solvents

^aIsolated yield

Table 3 Comparison of the efficiency of NiO@g-C₃N₄ with different catalysts

| Entry | Catalyst | Solvent/T (°C) | Time (min) | Yield (%) | References |
|-------|--|----------------------------|------------|-----------|------------|
| 1 | [CHOSO ₃ H] ₃ W ₁₂ PO ₄₀ | EtOH/r.t. | 40 | 92 | [12] |
| 2 | TBA acetate | Solvent-free/100 °C | 10 | 92 | [29] |
| 3 | (SB-DBU)Cl | EtOH/r.t. | 150 | 97 | [30] |
| 4 | Carbon-SO ₃ H | EtOH/reflux | 180 | 81 | [31] |
| 5 | Piperidine | EtOH/r.t. | 60 | 92 | [32] |
| 6 | Sodium citrate | H ₂ O/60 °C | 180 | 95 | [33] |
| 7 | NaOAc | Grinding | 15 | 95 | [34] |
| 8 | Urea: ChCl | Deep eutectic solvent | 60 | 95 | [35] |
| 9 | a-amilase | EtOH/H ₂ O/r.t. | 180 | 98 | [36] |
| 10 | TEBA | H ₂ O/60 °C | 180 | 90 | [37] |
| 11 | NiO@g-C ₃ N ₄ | EtOH/reflux | 2 | 95 | This work |

Reaction conditions: isatin (1 mmol), malononitrile (1 mmol) and dimedone (1 mmol)

Different methods have been reported for the synthesis of spirooxindole derivatives under different conditions [11, 27–35]. The method presented in this article has advantages over previous studies, including easy synthesis, short reaction time, workup and no side products (Table 3).

To show the generality of NiO@g-C₃N₄ in organic reactions, the synthesis of various spirooxindole derivatives using isatins and cyclic-1,3-diketone or 1,3-diketone esters or 4-hydroxycoumarin derivatives (Scheme 1) was investigated using the described reaction conditions (Table 4). Changing of substitutions on isatin caused the change in reaction time or yield (%), electron donating group on the R¹ or R² position reduce the reaction's progress (Table 4, entries 4, 5, 9, 17, 19 and 20), and electron withdrawing group (EWG) in the R² position increase the reaction speed and yield (%) (Table 4, entries 2, 3, 15 and 16). Studies have also shown that the dimedone can produce better results than 1,3-cyclohexadione (Table 4, entries 10–13). Also, studies have shown that the methyl and ethyl acetoacetate can produce various spirooxindole derivatives with less reactivity to dimedone (Table 4, entries 14–17). When 4-hydroxycoumarin was used, the synthesis of corresponding spirooxindole was less reactive compared to when 1,3-diketones was used (Table 4, entries 18–26); this may be due to less reactivity of 4-hydroxycoumarin than 1,3-diketones. Of course, it should be considered in these reactions the presence of EWG on isatins also led to less time and more product percentages (Table 4, entries 19 and 20). Generally, the best efficiencies were obtained with dimedone and isatin bearing EWG on R² position (Table 4, entry 12).

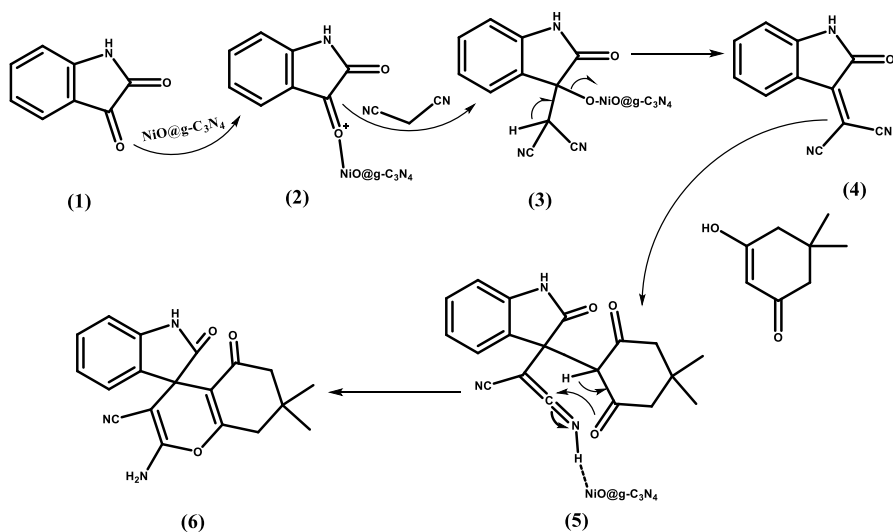
In all reactions, the products could easily be separated by recrystallizing in hot ethanol. As can be deduced from Table 4, no side products were produced in these reactions. Also, according to Table 4, NiO@g-C₃N₄ exhibited high catalytic activity, which could be due to the uniform distribution of NiO nanoparticles, which is stabilized by p-conjugated graphitic carbon nitrides as well as readily accessible surface-exposed NiO nanoparticles, which obviously favors the C–C bond formation reactions.

Table 4 Preparation of oxindole derivatives

| Entry | Isatin | | 1,3-diketone or 1,3-diketotoesters or 4-hydroxycoumarin | | Time (min) | Yield (%) |
|-------|-------------------------------|-----------------|---|----------------|------------|-----------|
| | R ¹ | R ² | R ³ | R ⁴ | | |
| 1 | H | H | H | – | 2 | 93 |
| 2 | H | Cl | H | – | 2 | 95 |
| 3 | H | NO ₂ | H | – | 2 | 95 |
| 4 | H | OMe | H | – | 3 | 90 |
| 5 | H | Me | H | – | 3 | 90 |
| 6 | C ₂ H ₅ | NO ₂ | H | – | 2 | 93 |
| 7 | C ₂ H ₅ | Br | H | – | 2 | 93 |
| 8 | Me | Br | H | – | 2 | 95 |
| 9 | CH ₂ Ph | H | H | – | 4 | 91 |
| 10 | CH ₂ Ph | H | Me | – | 4 | 93 |
| 11 | C ₂ H ₅ | NO ₂ | Me | – | 2 | 95 |
| 12 | H | Cl | Me | – | 2 | 97 |
| 13 | H | H | Me | – | 2 | 95 |
| 14 | H | H | – | Me | 6 | 92 |
| 15 | H | Me | – | Me | 8 | 90 |
| 16 | H | H | – | Et | 6 | 90 |
| 17 | H | Me | – | Et | 8 | 90 |
| 18 | H | H | – | – | 6 | 90 |
| 19 | H | Cl | – | – | 5 | 91 |
| 20 | H | NO ₂ | – | – | 5 | 93 |
| 21 | CH ₂ Ph | H | – | – | 7 | 88 |
| 22 | CH ₂ Ph | NO ₂ | – | – | 6 | 89 |
| 23 | H | OMe | – | – | 8 | 87 |
| 24 | H | Me | – | – | 8 | 88 |
| 25 | Me | Br | – | – | 7 | 90 |
| 26 | C ₂ H ₅ | Br | – | – | 7 | 80 |

Reaction conditions: isatin derivatives (1.0 mmol), 1,3-diketone or 1,3-diketotoesters or 4-hydroxycoumarin (1 mmol), malononitrile (1 mmol), catalyst (50 mg) and EtOH (3 mL); reactions conducted in reflux conditions

A plausible mechanism for one-pot reaction of isatin, dimedone and malononitrile is given in Scheme 3. As can be seen, the product of the first step is caused by the addition of NiO@g-C₃N₄ to the carbonyl group of isatin. Adding malononitrile to mentioned carbon, followed by the release of NiO along with the oxygen of the carbonyl group, produces 4. With the addition of dimedone, the NiO@g-C₃N₄ catalyst again enters to the mechanism to create 6 (spirooxindole derivatives).



Scheme 3 Proposed mechanism for the synthesis of spirooxindole derivatives

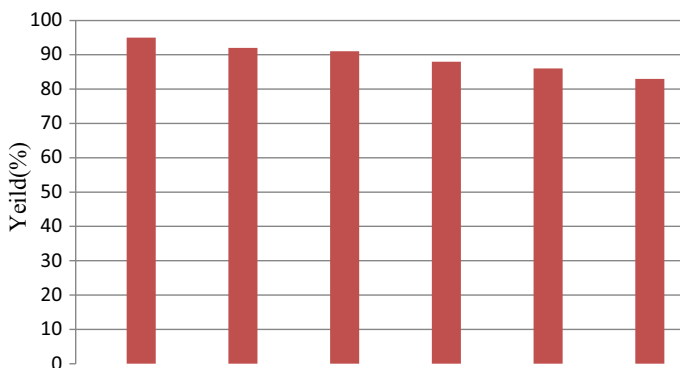


Fig. 5 Reusability of the NiO@g-C₃N₄ nanocomposite for the synthesis of spirooxindole derivatives

Since the reusability of the catalyst in the industry is important, repetitive experiments were conducted under similar conditions to investigate the stability of NiO@g-C₃N₄. So, after the end of each reaction, the catalyst was separated, washed and dried for subsequent use. After 6 times of catalyst reuse, the reaction efficiency was still above 80% which confirmed the catalyst recovery capability (Fig. 5).

Conclusion

We presented a rapid and green hydrothermal method for the immobilization of the NiO nanoparticles on the g-C₃N₄ nanosheets. Prepared nanocomposite was characterized by different techniques including TEM, XRD, TGA and FT-IR spectra. The one-pot synthesis of spirooxindole derivatives using 1 mmol isatin, 1 mmol dimedone and 1 mmol malononitrile was carried out in the presence of 50 mg NiO@g-C₃N₄ in EtOH media at reflux conditions. High percentage of products (90–97%) were produced in short reaction times (2–4 min). 4-Hydroxycoumarin was reacted instead of dimedone, and again acceptable results were obtained in terms of reaction times (5–8 min) with good reaction efficiency (87–93%). In addition, the catalyst stability was investigated for 8 cycles without a significant reduction in catalytic efficiency. Therefore, this study introduces a facile and green method for the synthesis of the NiO@g-C₃N₄ nanocomposite which can be effective for the synthesis of spirooxindole derivatives.

Acknowledgements The authors are grateful to the University of Birjand and Payam Noor University of Mashhad for financial support.

References

1. I.O. Ghinea, R.M. Dinica, New synthetic pathways, new applications, in *Scope of Selective Heterocycles from Organic and Pharmaceutical Perspective*, ed. by R. Varala (InTech, Rijeka, 2017), p. 115
2. I.V. Borovlev, O.P. Demidov, G.A. Amangasieva, E.K. Avakyan, N.A. Kurnosova, J. Heterocycl. Chem. **406**, 54 (2016)
3. N. Azizi, E. Gholibeghlo, Z. Manocheri, Sci. Iran. **19**, 574 (2012)
4. S. Budde, J.K. Ega, B. Gavaji, R. Vadde, Int. J. Res. Appl. **2**, 365 (2015)
5. G. Mohammadi Ziarani, R. Moradi, A. Badiiei, N. Lashgari, B. Moradi, A. Abolhasani Soorki, J. Taibah Univ. Sci. **9**, 555 (2015)
6. K. Rad-Moghadama, S. Gholizadeh, IJC **4**, 41 (2014)
7. F.X. Felpin, O. Iburguren, L. Nassar-Hardy, E. Fouquet, J. Org. Chem. **74**, 1349 (2009)
8. J. Kothandapani, A. Ganesan, G.K. Mani, A.J. Kulandaiamy, J.B. Balaguru Rayappan, S.S. Ganesan, Tetrahedron Lett. **57**, 3472 (2016)
9. A. Allahresani, Iran. J. Catal. **7**, 293 (2017)
10. J.A. Makawana, C.B. Sangani, Y.F. Yao, Y.T. Duan, P.C. Lv, H.L. Zhu, Mini Rev. Med. Chem. **16**, 1303 (2016)
11. M.A. Nasser, F. Kamali, B. Zakerinasab, RSC Adv. **5**, 26517 (2015)
12. J.A. Tanna, R.G. Chaudhary, N.V. Gandhare, A.R. Rai, H.D. Juneja, IJSER **6**, 93 (2015)
13. R.J. Kalbasi, N. Mosaddegh, Bull. Korean Chem. Soc. **32**, 2584 (2011)
14. L.L. Chng, N. Erathodiyil, J.Y. Ying, Acc. Chem. Res. **46**, 1825 (2013)
15. H. Sachdeva, D. Dwivedi, R.R. Bhattacharjee, S. Khaturia, R. Saroj, J. Chem. **2013**, 1 (2013)
16. X. Miao, X. Shen, J. Wu, Z. Ji, J. Wang, L. Kong, M. Liu, C. Song, Appl. Catal. A Gen. **539**, 104 (2017)
17. H. Liu, Z. Xu, Z. Zhang, D. Ao, Appl. Catal. A Gen. **518**, 150 (2016)
18. L. Ge, C. Han, J. Liu, Y. Li, Appl. Catal. A Gen. **409–410**, 215 (2011)
19. Q. Hao, X. Niu, C. Nie, S. Hao, W. Zou, J. Gea, D. Chen, W. Yao, Phys. Chem. Chem. Phys. **18**, 31410 (2016)
20. B. Lin, C. Xue, X. Yan, G. Yang, G. Yang, Appl. Surf. Sci. **357**, 346 (2015)

21. L.C. Chen, X.T. Zeng, P. Si, Y.M. Chen, Y.W. Chi, D.H. Kim, G. Chen, *Anal. Chem.* **86**, 4188 (2014)
22. A. Thomas, A. Fischer, F. Goettmann, M. Antonietti, J.-O. Müller, R. Schlogl, J.M. Carlsson, *J. Mater. Chem.* **18**, 4893 (2008)
23. X. Wang, K. Maeda, A. Thomas, K. Takanabe, *Nat. Mater.* **8**, 76 (2009)
24. B. Long, J. Lin, X. Wang, *J. Mater. Chem. A* **2**, 2942 (2014)
25. A. Allahresani, B. Taheri, M.A. Nasser, *Res. Chem. Intermed.* **44**, 6979 (2018)
26. A. Allahresani, B. Taheri, M.A. Nasser, *Res. Chem. Intermed.* **44**, 1173 (2018)
27. A. Allahresani, M.A. Nasser, A. Nakhai, *Res. Chem. Intermed.* **43**, 6367 (2017)
28. S. Riyaz, A. Indrasena, A. Naidu, P.K. Dubey, *Indian J. Chem. B* **53**, 1442 (2014)
29. R.Y. Guo, Z.M. An, L.P. Mo, S.-T. Yang, H.-X. Liu, S.-X. Wang, Z.-H. Zhang, *Tetrahedron* **69**, 9931 (2013)
30. C. Wu, R. Shen, J. Chen, C. Hu, *Bull. Korean Chem. Soc.* **34**, 2431 (2013)
31. S.P. Sataia, P.N. Kalaria, J.R. Avalani, D.K. Raval, *Tetrahedron* **70**, 5763 (2014)
32. P. Rai, M. Srivastava, J. Singh, J. Singh, *New J. Chem.* **38**, 3181 (2014)
33. A. Hasaninejad, N. Golzar, M. Beyrati, A. Zare, M.M. Doroodmand, *J. Mol. Catal. A Chem.* **372**, 137 (2013)
34. L.-M. Wang, N. Jiao, J. Qiu, J.-J. Yu, J.-Q. Liu, F.-L. Guo, Y. Liu, *Tetrahedron* **66**, 339 (2010)
35. M.N. Elinson, R.F. Nasybullin, F.V. Ryzhkov, T.A. Zaimovskaya, G.I. Nikishi, *Monatsh. Chem.* **146**, 631 (2015)
36. S.J. Chai, Y.F. Lai, J.C. Xu, H. Zheng, Q. Zhu, P.F. Zhang, *Advanc. Synth. Catal.* **353**, 371 (2011)
37. L. Zhao, B. Zhou, Y. Li, *Heteroatom Chem.* **22**, 673 (2011)

Publisher's Note Springer Nature remains neutral with regard to jurisdictional claims in published maps and institutional affiliations.